Steady shape analysis of tomographic pumping tests for characterization of aquifer heterogeneities

Geoffrey C. Bohling, Xiaoyong Zhan, James J. Butler Jr., and Li Zheng

Kansas Geological Survey, University of Kansas, Lawrence, Kansas, USA

[1] Hydraulic tomography, a procedure involving the performance of a suite of pumping tests in a tomographic format, provides information about variations in hydraulic conductivity at a level of detail not obtainable with traditional well tests. However, analysis of transient data from such a suite of pumping tests represents a substantial computational burden. Although steady state responses can be analyzed to reduce this computational burden significantly, the time required to reach steady state will often be too long for practical applications of the tomography concept. In addition, uncertainty regarding the mechanisms driving the system to steady state can propagate to adversely impact the resulting hydraulic conductivity estimates. These disadvantages of a steady state analysis can be overcome by exploiting the simplifications possible under the steady shape flow regime. At steady shape conditions, drawdown varies with time but the hydraulic gradient does not. Thus transient data can be analyzed with the computational efficiency of a steady state model. In this study, we demonstrate the value of the steady shape concept for inversion of hydraulic tomography data and investigate its robustness with respect to improperly specified boundary conditions.   *INDEX TERMS:* 1829 Hydrology: Groundwater hydrology; 1894 Hydrology: Instruments and techniques; 3260 Mathematical Geophysics: Inverse theory; *KEYWORDS:* hydraulic tomography, aquifer characterization

1. Introduction

[2] Pumping and slug tests are the most commonly used field techniques for characterizing the transmissive properties of an aquifer. Unfortunately, when the focus of an investigation is on contaminant transport, the information provided by these techniques is often of relatively limited value. Conventional pumping tests yield hydraulic conductivity (K) estimates that represent an average over a relatively large volume of an aquifer [*Butler*, 1990; *Butler and Liu*, 1993; *Meier et al.*, 1998]. Contaminant transport, however, is sensitive to the manner in which hydraulic conductivity varies in space and, particularly, to the spatial arrangement of laterally continuous regions of extreme values. Slug tests can provide information about spatial variations in K at a scale of relevance for transport investigations [*Yeh et al.*, 1995], but the parameter estimates are subject to significant bias as a result of incomplete well development [*Butler*, 1998; *Butler and Healey*, 1998]. Furthermore, conventional slug tests, which only use measurements in the test well, are not capable of yielding information about the continuity of layers between wells. Clearly, new approaches are needed if hydraulic tests are to provide information of more significance for transport investigations.

[3] Over the last decade, several research groups have begun work on a new hydraulic test method, known as hydraulic tomography, that has the potential to yield a detailed description of spatial variations in hydraulic conductivity between wells [*Bohling*, 1993; *Tosaka et al.*, 1993; *Gottlieb and Dietrich*, 1995; *Butler et al.*, 1999; *Yeh and Liu*, 2000]. As shown in Figure 1, this approach essentially consists of a series of short-term pumping tests in which the position of the stressed interval in the pumping well, isolated with packers, is varied between tests. In each test, the aquifer is "probed" by a streamline configuration that converges on a different pumping interval. The sequence of tests produces a pattern of crossing streamlines in the region between the pumping and observation wells similar to the pattern of crossed ray paths used in seismic or radar tomography [*Peterson et al.*, 1985; *Vasco et al.*, 1997]. Although a large number of drawdown measurements is required to delineate the numerous streamlines produced by the test sequence, new methods for drawdown measurement have been developed that can provide the requisite density of data in a practically feasible manner [*Butler et al.*, 1999].

[4] The primary objective of this paper is to present an efficient and robust approach for the analysis of drawdown data from hydraulic tomography experiments. The field methods presented by *Butler et al.* [1999] do reduce the time and expense involved with the field implementation of the tomography procedure. These methods, however, are of practical utility only if they can be coupled with efficient means for analysis of the drawdown data. Most previously proposed methods for drawdown analysis have assumed steady state conditions [*Bohling*, 1993; *Yeh and Liu*, 2000], but reliance on steady state conditions severely limits the
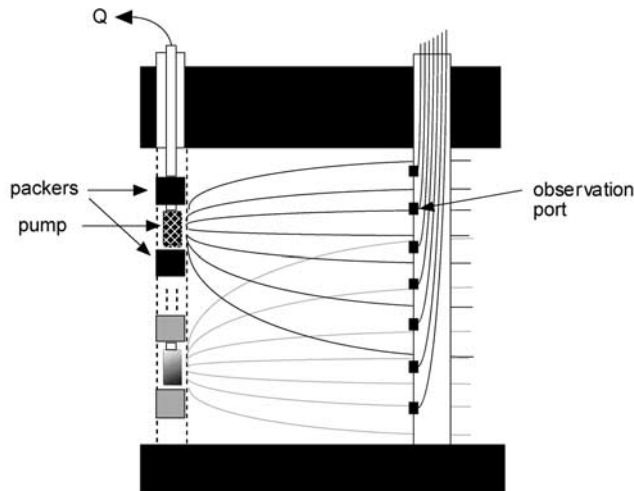
Figure 1. Schematic representation of two tests in a sequence of pumping tests in tomographic format with lines representing converging streamline patterns for each test.

utility of such methods. For example, attainment of steady state conditions often requires many hours, if not days, of pumping, a duration that would not be feasible for practical applications. Moreover, a steady state analysis requires assumptions about the boundary conditions controlling the transition of the flow system to steady state, an issue that is usually the source of considerable uncertainty. The propagation of that uncertainty will often have a significant impact on K estimates.

[5] *Vasco et al.* [2000] propose an approach that has potential to greatly increase the efficiency of the analysis of data from pumping tests in tomographic format. This technique involves identifying and matching the arrival times of the peak slope of the drawdown-versus-time curve at different locations. However, the approach does have some significant limitations. First, arrival times are primarily controlled by the aquifer diffusivity (ratio of hydraulic conductivity to specific storage), making it difficult to separate the effects of conductivity and storage. Second, identifying peak slope arrival times requires use of early-time drawdown data that can be affected by a variety of nonideal mechanisms (e.g., inertia-induced mechanisms in highly permeable systems [*Shapiro*, 1989]) that have an insignificant impact on drawdown data at larger times.

[6] The analysis approach introduced in this paper avoids the limitations of these previous methods by exploiting the simplifications possible under a flow regime known as steady shape, unsteady state [*Heath and Trainer*, 1968; *Butler*, 1990]. This steady shape concept, which has its origins in the early work of *Theis* [1940] on the nature of pumping-induced drawdown, enables transient drawdown data to be analyzed with a steady state model. Transient data can be processed with the computational efficiency of a steady state model, while avoiding the errors introduced by inappropriate assumptions about the boundary conditions driving the system to steady state or the nonidealities associated with early-time data. When combined with the field methods described by *Butler et al.* [1999], the new analysis approach should greatly enhance the practical viability of the hydraulic tomography methodology.

[7] This paper will describe the steady shape analysis method and demonstrate its efficacy in a series of numerical experiments using a synthetic, imperfectly layered aquifer. The paper begins with an overview of the steady shape concept followed by a description of the numerical approaches used to generate and analyze drawdown from a series of simulated tests. The computed drawdowns are analyzed with transient, steady state, and steady shape inversion techniques. The K estimates from these analyses are compared to the hydraulic conductivity values used as inputs for the test simulations to assess the viability of the various approaches. The dependence of the steady state and steady shape approaches on the assumed mechanism responsible for steady state conditions is also examined. The paper concludes with an assessment of the sensitivity of the steady shape approach to the number of drawdown measurements and to the magnitude of measurement error.

2. Steady Shape Flow Regime

[8] The term steady shape, unsteady state (henceforth steady shape) is used to designate conditions, common to both confined and unconfined aquifers, in which drawdown is continuing to change with time but the hydraulic gradient is not. These conditions have also been described as steady radial flow [*Jacob*, 1963] and transient steady state flow [*Kruseman and de Ridder*, 1989]. Figure 2 displays a field example of the steady shape conditions observed during preliminary tests of the hydraulic tomography concept. As shown in Figure 2 and elsewhere [e.g., *Kruseman and de Ridder*, 1989, Figure 3.3], steady shape conditions are established very rapidly in many field settings. *Theis* [1940] states that the establishment of these conditions is an indication that those portions of the aquifer are providing an insignificant contribution to well discharge and are merely serving as conduits for the transportation of water from more distant regions. *Butler* [1988], following on earlier work by *Wenzel* [1942], discusses how steady shape conditions can be exploited to use the Thiem equation to analyze transient drawdown data. He also derives a simple analytical solution [*Butler*, 1988, equation 24] to prove that the hydraulic gradients under steady shape conditions are the same as those that will exist under true steady state conditions, if those conditions are ever achieved. The proof of *Butler* [1988] was developed for radially symmetric flow conditions but the equivalence also holds for higher dimensions, as can easily be demonstrated numerically.

[9] The equivalence of hydraulic gradients at steady state and steady shape conditions serves as the theoretical basis of the analysis approach described in this paper. This equivalence allows drawdown data from a set of hydraulic tomography experiments to be analyzed using a steady state model, even though the flow system may be far from attainment of true steady state conditions (e.g., Figure 2). The practical field ramifications of this equivalence are profound, as the time to complete a suite of tomography experiments can be decreased by orders of magnitude from that required when true steady state conditions must be attained (decrease between three to four orders of magnitude for the aquifer of Figure 2). *Butler* [1988] shows that the time at which steady shape conditions are achieved corresponds to the time at which the semilog approximation of *Cooper and Jacob* [1946] becomes valid ($t > 100 \ r^2 S/4T$ for
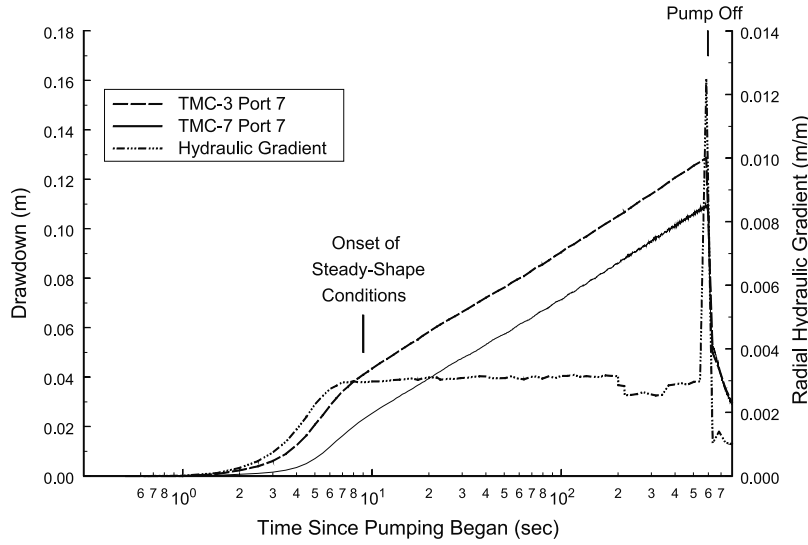
Figure 2. Drawdown versus logarithm of time plot for 12 August 1997 pumping test 1 (drawdown measured in ports of multilevel sampling wells using approach of *Butler et al.* [1999]; multilevel sampling wells TMC-3 and TMC-7 are positioned along a ray at distances of 4.6 m and 10.7 m, respectively, from the pumping well; decrease in the magnitude of the hydraulic gradient between 200–400 s thought to be a product of backpressure changes associated with flow rate measurements).

pumping from a well fully screened across a confined aquifer, where r is distance from pumping well, S is storativity, and T is transmissivity). Thus, as shown in Figure 2, the time will be on the order of seconds to tens of seconds for regions in the immediate vicinity of the pumping well.

[10] The ramifications of this equivalence for the data analysis phase of the hydraulic tomography procedure are also profound, as the time to complete a steady shape analysis of a set of tomography experiments is significantly less than that needed for a formal transient analysis. In addition, because no assumptions are invoked concerning the boundary conditions leading to steady state, the steady shape approach is significantly more accurate than a true steady state analysis.

[11] This second set of issues, the computational and accuracy gains possible with a steady shape approach, will be the primary focus of the remainder of this paper. A radial-coordinate numerical model will be used to demonstrate the advantages of a steady shape approach over conventional transient and steady state analyses for a variety of scenarios associated with tests in permeable alluvial aquifers. The numerical model and the parameter estimation methodology used in the analysis of the simulated drawdown are briefly described in the following section.

3. Model and Parameter Estimation Overview

[12] The simultaneous analysis of drawdown data from multiple pumping tests was done here using lr2dinv, a radial-coordinate finite difference flow model described by *Bohling and Butler* [2001]. Assuming flow to a pumping well under confined conditions and symmetry in the angular direction, the hydraulic head, h [L], at a point with radial coordinate r [L], whose origin is at the center of the well, and vertical coordinate z [L], is governed by the equation:

$$\frac{1}{r}\frac{\partial}{\partial r}\left(rK_r\frac{\partial h}{\partial r}\right) + \frac{\partial}{\partial z}\left(K_z\frac{\partial h}{\partial z}\right) = S_s\frac{\partial h}{\partial t} \qquad (1)$$

where K_r [L/T] is the radial hydraulic conductivity, K_z [L/T] is the vertical hydraulic conductivity, S_s is specific storage [L^{-1}], and t [T] is time. The radial flow equation can be cast in an equivalent Cartesian form by introducing the logarithmically transformed radial coordinate $r' = \ln(r/r_w)$, where r_w is the pumping well radius, yielding

$$\frac{\partial}{\partial r'}\left(K_r\frac{\partial h}{\partial r'}\right) + \frac{\partial}{\partial z}\left(K_z'\frac{\partial h}{\partial z}\right) = S_s'\frac{\partial h}{\partial t} \qquad (2)$$

with

$$K_z' = r^2 K_z = r_w^2 e^{2r'} K_z \text{ and } S_s' = r^2 S_s = r_w^2 e^{2r'} S_s.$$

Lr2dinv solves Equation 2 on a rectangular finite difference grid with a constant vertical spacing, Δz, and a constant spacing, $\Delta r'$, in the transformed radial direction, yielding exponentially increasing cell widths with increasing radial cell index. Thus the radial variation in the hydraulic conductivity field is represented in great detail near the pumping well and in a very coarse fashion far from it. Although this discretization scheme may appear to introduce an artificial bias into the analysis, this telescoping view of aquifer heterogeneity actually reflects the physics of the radial flow process. As described by *Butler* [1990] and *Butler and Liu* [1993], the sensitivity of pumping-induced drawdown to the hydraulic conductivity of a fixed volume of aquifer decreases rapidly with increasing separation between the pumping well and the portion of aquifer in question. The exponentially increasing radial increment therefore incorporates this loss of sensitivity to detail with increasing radial distance. Although drawdown at an observation well will show some sensitivity to nearby conductivity variations [*Oliver*, 1993], that drawdown will be sensitive only to the bulk properties, not the detailed variations, of material beyond a certain radial distance outward from that region.
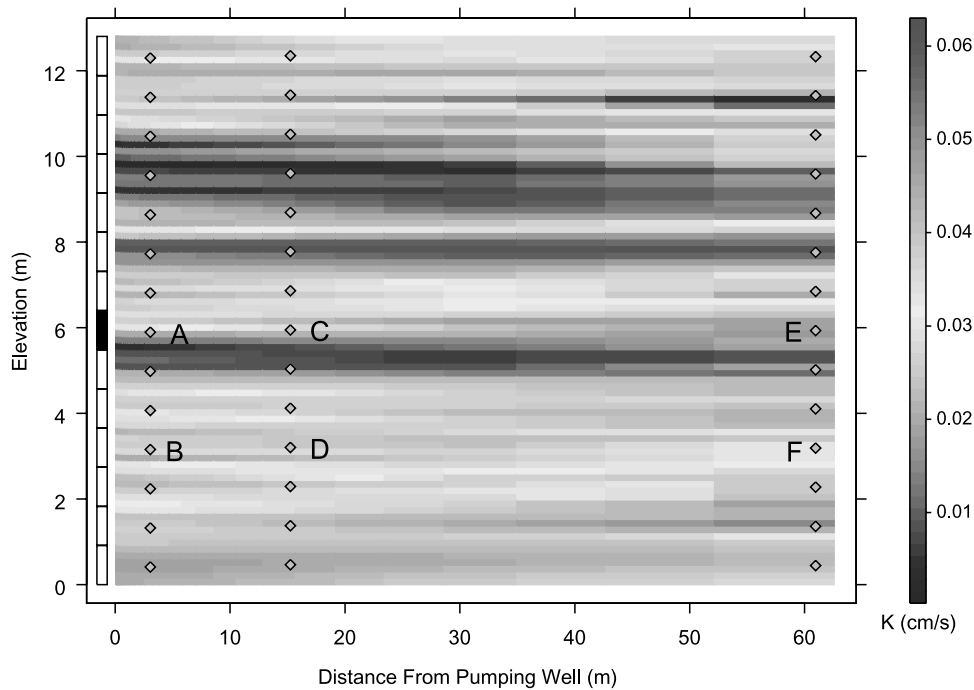
Figure 3. True conductivity distribution out to 62 m radial distance from pumping well. Boxes on left indicate pumping intervals for 14 tests, with interval for test 7 highlighted. Diamonds represent observation points. Drawdowns at points A−F are shown in following figures. See color version of this figure at back of this issue.

[13] For parameter estimation, lr2dinv employs the Levenberg-Marquardt algorithm [*Marquardt*, 1963] as implemented in the public domain code lmdif [*Garbow et al.*, 1980]. Lr2dinv allows independent, arbitrary zonations of parameters over the model grid. The critical aspect of the inversion process for hydraulic tomography is the ability to simultaneously analyze responses from multiple tests. Lr2dinv accomplishes this quite simply by simulating the entire suite of tests based on the current parameter estimates and then collecting the discrepancies between observed and predicted drawdowns from all tests into a single vector of residuals. This vector of residuals is passed back to the Levenberg-Marquardt code, which is unaffected by the details of the process generating the residuals.

[14] For the steady shape simulations of this study, lr2dinv was modified to allow parameter estimation based on differences of drawdown between observation points rather than absolute values of drawdown. As will be shown, this allows efficient analysis of data collected during the "steady shape" phase of a pumping test.

4. Generation of Synthetic Data

[15] Synthetic drawdown data were generated by running lr2dinv in forward mode with a known, heterogeneous distribution of hydraulic conductivity. Flow properties were chosen to approximate what one might expect to find in an alluvial sand and gravel aquifer, with relatively high conductivity values following a distribution characterized by a significant degree of horizontal continuity. The model aquifer is 12.8 m thick, with an overall average horizontal hydraulic conductivity of 2.2×10^{-4} m/s (a value characteristic of clean sand [*Freeze and Cherry*, 1979]). A specific

storage value of 9.8×10^{-6} m^{-1} was used for all cells. For the sake of forward modeling, the model domain was discretized into 84 cells in the vertical, each 0.15 m thick, and 60 nodes in the radial direction, with an increment of $\Delta \ln(r/r_w) = 0.2$ in the transformed radial dimension. The pumping well radius (r_w) is 0.0706 m, implying that the outer boundary of the model domain is at $r_w \exp(60 * 0.2) = 11,492$ m. Figure 3 shows the synthetically generated "true" horizontal conductivity distribution out to a distance of 62 m (34 nodes in the radial direction) from the pumping well. The diamonds on the plot represent the locations of 42 observation points, in three vertical lines of 14 observation points each at 3, 15, and 61 m from the pumping well. The heterogeneous conductivity distribution continues to the outer boundary, but comparisons between true and estimated conductivities will focus on the region shown, which is designated the "region of investigation". The bulk conductivity outside this region controls the gradient between the outer boundary and the region of investigation, but the details of the conductivity distribution outside this region have little influence on the results reported here.

[16] Simulations were performed using two different spatially constant values for the ratio of vertical to horizontal hydraulic conductivity, representing two bounding cases. In one set of simulations, an anisotropy ratio of 1 was employed, meaning that the conductivity for each model cell was considered to be isotropic. In another set of simulations, the model cells were considered to be strongly anisotropic, with an anisotropy ratio of 1.0×10^{-3}, a value that would not be expected unless the 0.15-m thick cells typically incorporated a number of thin clay layers.

[17] The rectangles along the left side of Figure 3 represent the pumping intervals, each 0.9-m in length, for fourteen
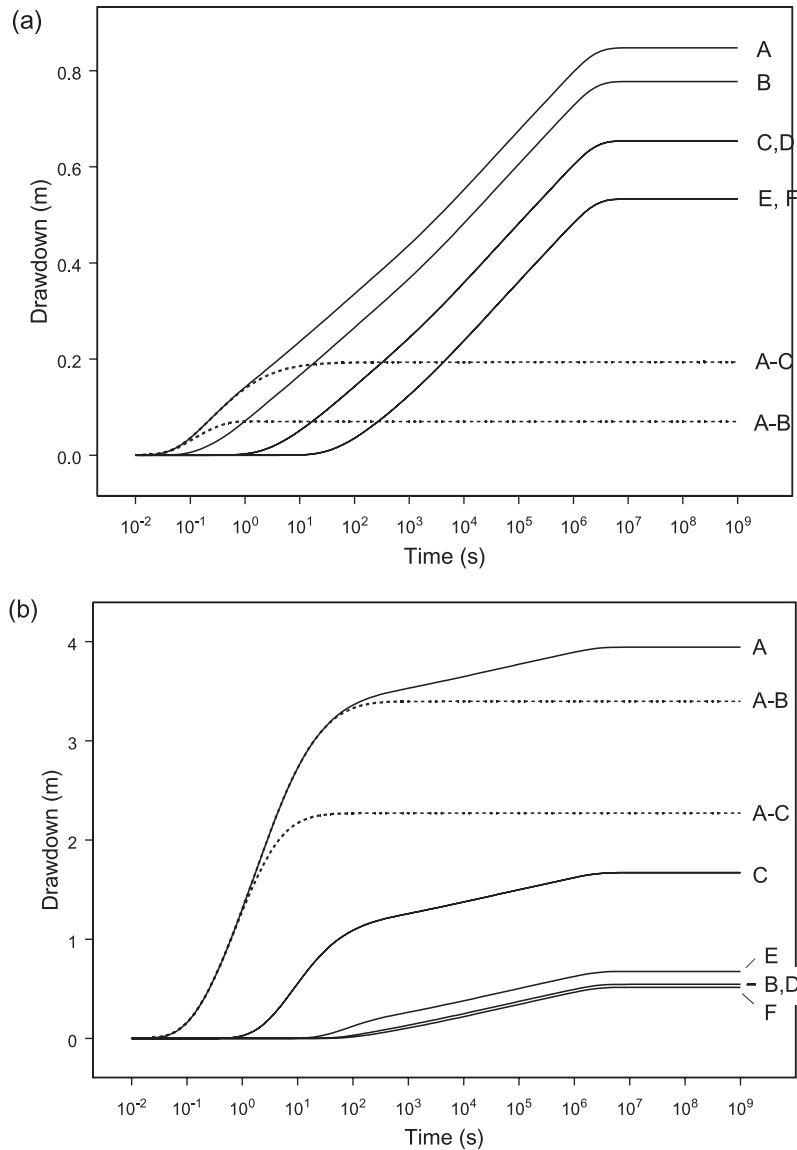
Figure 4. Responses at six observation points (A−F in Figure 3) for test seven with anisotropy ratios of (a) $K_z:K_r = 1.0$ and (b) $K_z:K_r = 1.0 \times 10^{-3}$.

different pumping tests. The pumping rate for each test was 1.89 L/s. Simulations were run with an initial condition of zero drawdown throughout the model domain, no-flow upper and lower boundary conditions, and a zero-drawdown (constant-head) outer boundary condition. The filled rectangle represents the pumping interval for the seventh test. Figure 4a shows drawdown responses for this test at the six labeled observation points (A through F) for the simulations using an anisotropy ratio of 1.0, while Figure 4b shows the responses for an anisotropy ratio of 1.0×10^{-3}. The presence of a constant-head outer boundary implies that the system must eventually reach steady state, but this does not occur until after about 3×10^6 s (35 days), due to the great distance (11.5 km) to the outer boundary. In other words, this system does not reach steady state conditions within any practical time frame. However, for both anisotropy values, the system achieves a steady shape configuration, characterized by constant and parallel slopes of plots of drawdowns versus log time, within 1000 s (17 min).

[18] Under conditions of pumping a well fully screened across an equivalent homogeneous aquifer with a conductivity of 2.2×10^{-4} m/s and specific storage of 9.8×10^{-6} m^{-1}, the Cooper-Jacob criterion would be satisfied after about 10 s at the 3-m radius (points A and B), 260 s at the 15.2-m radius (points C and D), and 4100 s at the 61-m radius. The partially-penetrating nature of the flow and aquifer heterogeneity modify the time to onset of steady shape conditions, but a constant slope of drawdown versus log time is still achieved within a practical time frame at all locations. After this point, the differences in drawdown between observation points in the tested region are constant. The dashed lines on Figures 4a and 4b show the differences in drawdown between points A and B and between A and C, demonstrating that constant drawdown differences between these points are obtained within about 10 s under isotropic conditions and within about 100 s under anisotropic conditions. The steady shape approach to inversion focuses directly on such drawdown differences, which are
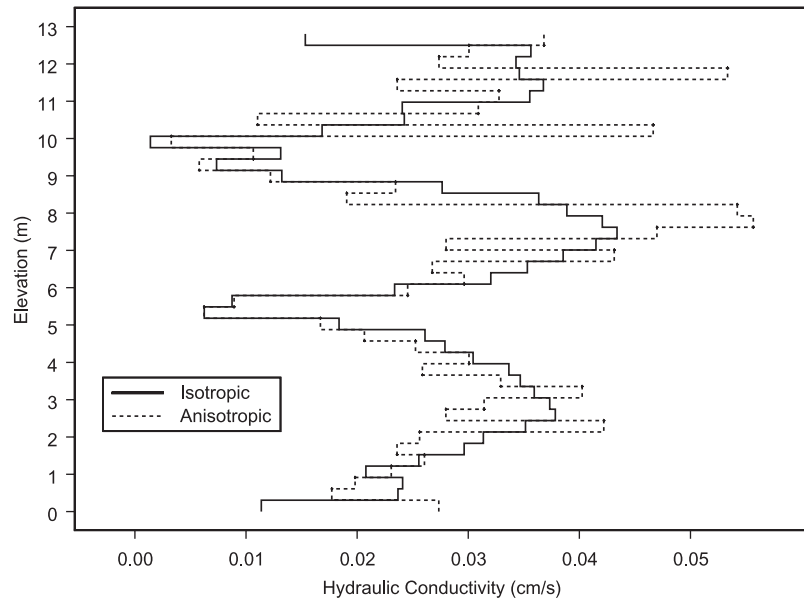
Figure 5. Hydraulic conductivity estimates from transient inversions under isotropic and anisotropic conditions.

solely a function of energy losses between the observation points, rather than the drawdown, which is also a function of conditions outside the region of investigation.

[19] The coincidence of drawdown at points C and D and points E and F on Figure 4a shows that under isotropic conditions vertical drawdown gradients dissipate rapidly with increasing distance from the pumping well, indicating that the responses under isotropic conditions provide significantly less information about the conductivity distribution than do those under anisotropic conditions. In a homogeneous confined aquifer of thickness b with horizontal hydraulic conductivity K_r and vertical conductivity K_z, it is expected that effects of partial penetration will not be seen beyond a distance of approximately $1.5b\sqrt{K_r/K_z}$ from the pumping well [*Domenico and Schwartz*, 1990; *Hantush*, 1961], or approximately 19 m for a homogeneous, isotropic aquifer of the same thickness as the model aquifer (12.8 m). For the particular test and observation points shown in Figure 4a, the effects of partial penetration are negligible at the 15.2-m observation radius in the heterogeneous model aquifer.

5. Transient Inversion

[20] As a basis for comparison, a fully transient analysis of data from 14 tomographic pumping tests was performed. Each of these simulated tests was carried out to 1000 s (16.7 min) with 51 drawdown observations obtained at each sampling point over that time, for a total of 29,998 measurements over the 14 tests. The observations were logarithmically spaced in time, beginning at a time of 10^{-2} s. The objective function for the transient inversion is the sum of squared differences between observed and simulated drawdowns

$$J_{st} = \sum_{i=1}^{n} \left[d_i - \hat{d}_i \right]^2 \qquad (3)$$

where n is the total number of observations, d_i is the observed drawdown at the location and time indexed by i, and $\hat{d}_i$ is the corresponding predicted drawdown.

[21] The model grid used in all the inverse analyses employs the same radial discretization as that used to generate the synthetic data, but with forty-two 0.30-m thick cells in the vertical, as opposed to the eighty-four 0.15-m thick cells in the forward model. The coarser vertical discretization was introduced in part to reduce simulation times in the inverse analyses, but also to incorporate an inherent discrepancy between the model used for estimation and the "true" model used to generate the synthetic data. Although this discrepancy is simple and artificial compared to that existing between a model and reality, it at least encapsulates one of the most important model errors in aquifer simulation: the inability to resolve the detailed vertical variation of flow and transport properties.

[22] A further simplification for the inverse analyses is the use of a perfectly layered zonation (42 layers) for the conductivity distribution. Given a tomographic test setup, the sensitivity of the tests is primarily to hydraulic conductivity variations in the vertical direction. A perfectly layered zonation simply reflects this fundamental sensitivity behavior.

[23] Figure 5 shows the conductivity distribution estimated from the transient analysis of the tomographic tests, both under isotropic and anisotropic conditions. Overall, the estimated conductivities appear to match the true conductivities (Figure 3) quite well, within the limitations imposed by the perfectly layered zonation. Figure 6 depicts the relative error in the estimates for each cell in the forward model grid. That is, the 42 layer estimates obtained in the inverse analysis have been mapped back onto the finer grid of the forward model, and estimated and true conductivities compared on this finer grid. Clearly the patterns of over- and underestimation are quite similar for both anisotropy ratios. Throughout much of the aquifer, the ratio of estimated to true conductivity is near 1 (logarithm is near 0). The greatest discrepancies occur between about 10 and 11.5 m above datum, a region characterized by an alternation between thin high and low conductivity zones separated by
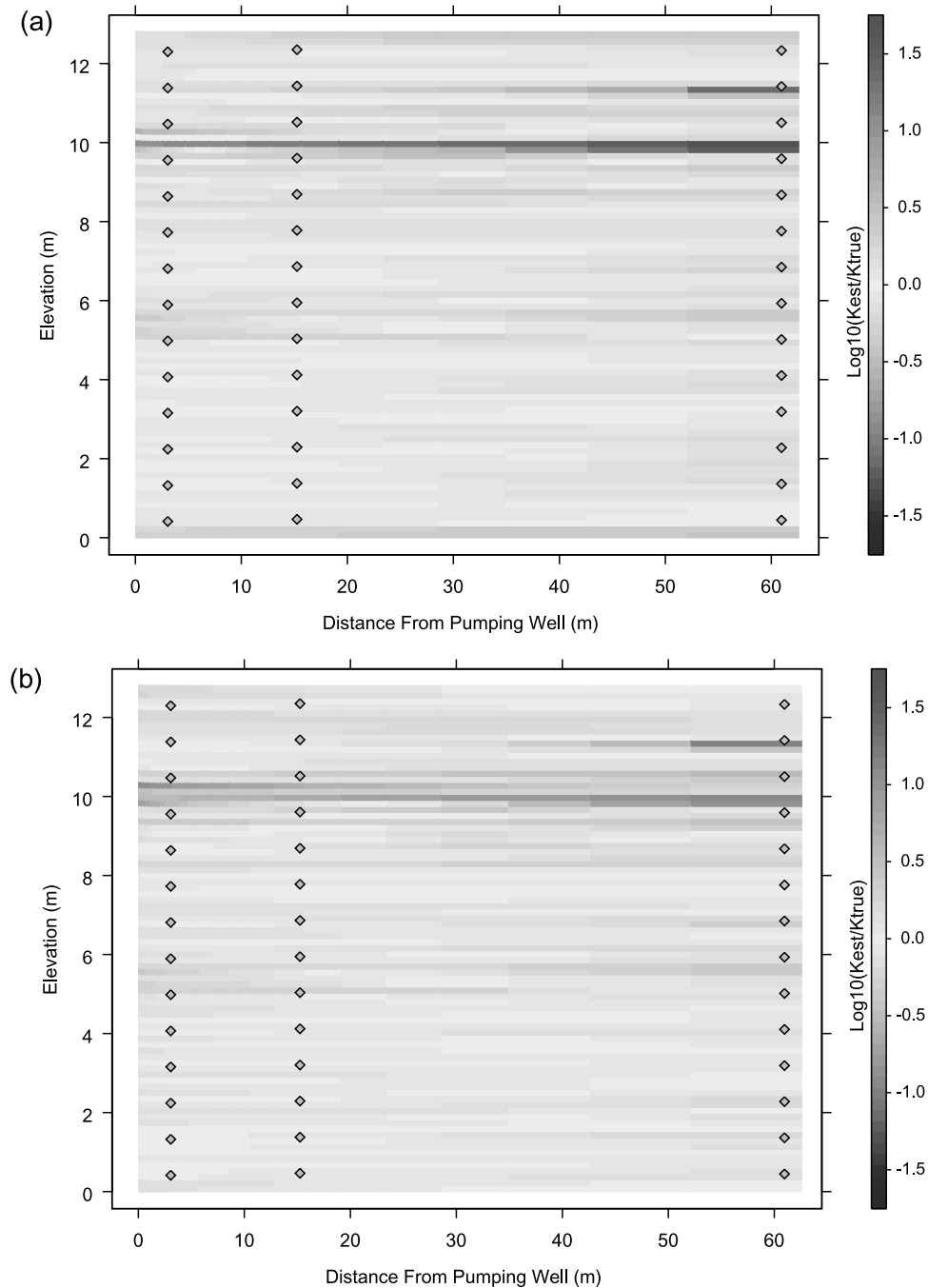
Figure 6. Relative error from transient inversions under (a) isotropic and (b) anisotropic conditions, represented in terms of the base 10 logarithm of estimated versus true conductivity in each cell of the forward model grid. See color version of this figure at back of this issue.

sloping boundaries. This variability cannot be adequately captured by the zonation used in the inverse analysis.

[24] Using four processors of an SGI Origin 2000, the transient inverse analysis required about 24 cpu hours for the isotropic case and about 14 cpu hours for the anisotropic case. Part of the reason for the difference in run times is that the preconditioned conjugate gradient algorithm used in the forward simulation program is sensitive to aquifer anisotropy. The preconditioning matrix is the tridiagonal matrix that would result from setting the vertical conductivity values to zero. Thus, as the degree of anisotropy increases (the vertical to horizontal conductivity ratio decreases), the preconditioning matrix becomes a more accurate approximation of the full coefficient matrix and fewer iterations are required to solve for drawdowns at each time step. In addition, the drawdown data obtained under anisotropic conditions are more sensitive to conductivity variations, due to the greater persistence of vertical gradients under anisotropic conditions. Therefore, under anisotropic conditions, fewer iterations of the Levenberg-Marquardt algorithm are required to obtain convergence. In either case, such computational demands present a challenge to the
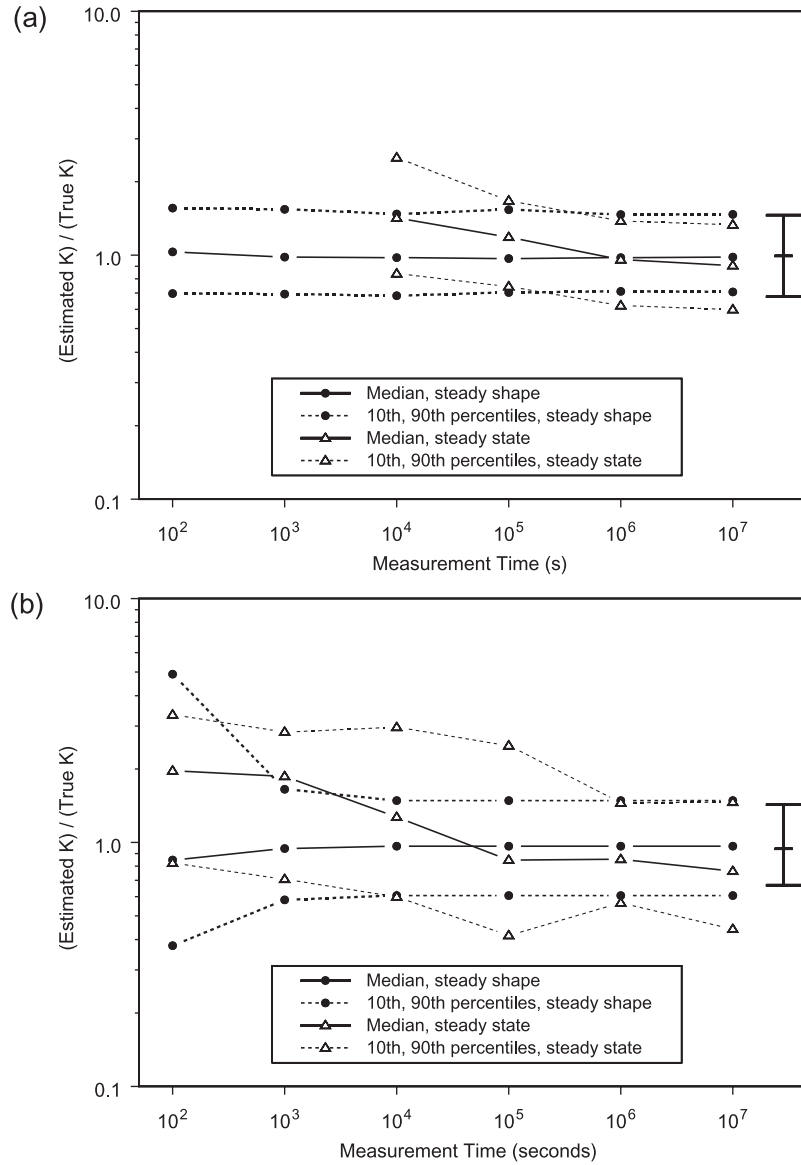
Figure 7. Summary of relative errors versus measurement time for steady state and steady shape inversions under (a) isotropic and (b) anisotropic conditions. Summaries of relative errors for corresponding transient inversions (based on tests of 1000-s duration) are shown to the right on each plot.

feasibility of this approach for the analysis of hydraulic tomography data. An obvious approach to reducing the computational demand is to perform steady state rather than transient simulations. The next section examines two approaches based on steady state simulations.

6. Steady State Versus Steady Shape Inversion

[25] Computation time can be reduced substantially by using steady state, rather than transient, simulations of the individual pumping tests, in which case the transformed governing equation is simply

$$\frac{\partial}{\partial r'}\left(K_r\frac{\partial h}{\partial r'}\right) + \frac{\partial}{\partial z}\left(K'_z\frac{\partial h}{\partial z}\right) = 0 \qquad (4)$$

and no time stepping is involved in the simulation. In the steady state approach, a single set of assumed steady state

observations is analyzed and no assumption is required about specific storage. The objective function for steady state inversion is the same as that for transient inversion (Equation 3), except that n is now the number of observation points at a single measurement time.

[26] Steady state analyses were carried out for measurement times ranging from 100 to 1×10^7 s, each based on the drawdown values observed at the 42 measurement points at that time. As with the transient inversions discussed above, a 42-layer zonation was used in the inversion and relative errors were computed on a cell-by-cell basis. Figure 7 summarizes the relative errors resulting from steady state analysis of the 14-test tomographic suite, in terms of the median and 10th and 90th percentiles of the ratio of estimated to true conductivity over the region of investigation (out to 62 m from the pumping well). The parameter estimates failed to converge for the 100- and 1000-s observation times under isotropic conditions because the system is

far from steady state. For the remaining cases, the computing time for each steady state inverse run was about 10 to 15 cpu min on the SGI Origin 2000, a speed-up of essentially two orders of magnitude relative to the transient inversions.

[27] Under the steady state assumption, the effect of the zero-drawdown outer boundary is propagated throughout the entire system instantaneously. However, in the actual system, the influence of the outer boundary is not felt until around 10^6 s (Figure 4). As shown in Figure 7, this leads to a considerable degree of overestimation in the conductivity values computed from the steady state analyses using data from times up to 10,000 s (2.8 hours). At these times, the observed drawdowns are lower than they would actually be under steady state conditions, leading to an underestimation of the overall gradient between the region of investigation and the outer boundary. In order to match the known flux value, the conductivities must increase to compensate for the artificially reduced gradient. The distribution of relative errors from the steady state analysis becomes more symmetrical about the ideal value of one for greater test times, but never quite stabilizes, even at extremely long test durations. This instability results from the use of drawdowns, which are affected by conditions outside the region of investigation, in the objective function. In short, the artificial influence of the outer boundary imposed by the assumption of steady state introduces significant errors in the conductivity estimates obtained from tests of reasonable duration.

[28] The values plotted as circles in Figure 7 are the relative errors resulting from steady shape analysis of the same data as in the steady state inversions. The steady shape analysis also involves a steady state simulation of each test in the tomographic suite. The only difference between steady state and steady shape analysis is that the objective function for the steady shape analysis is based on differences of drawdown between observation locations, rather than on the drawdowns themselves. The objective function for steady shape analysis is therefore the sum of the squared differences of observed and predicted drawdown differences between observation points

$$J_{sh} = \sum_{k=1}^{np} \left[\left(d_{i(k)} - d_{j(k)} \right) - \left(\hat{d}_{i(k)} - \hat{d}_{j(k)} \right) \right]^2 \qquad (5)$$

where np is the number of selected pairs of observation points and $i(k)$ and $j(k)$ represent the observation point indices for pair k. The results shown here use all possible pairs of observation points (861 pairs for the 42 observation points). As with the steady state analyses, the inverse runs for each analysis require approximately 10 to 15 cpu min on the SGI 2000.

[29] One might expect the steady state results of Figure 7 to converge to the steady shape results as the system approaches true steady state. At the moment we are not completely certain why there is still some discrepancy between the two sets of results at the final analysis time of 10^7 s. Apparently the use of different objective functions (Equations 3 and 5) induces the estimation algorithm to follow slightly different paths through parameter space, despite the theoretical equivalence of the two approaches in this case.

[30] Figure 8 shows the estimated conductivity values for the 42 layers based on the steady state and steady shape

analyses of data collected at 1000 s (10,000 s for the steady state analysis under isotropic conditions, due to the lack of convergence at earlier times), together with the transient analysis of data collected out to 1000 s. The overestimation of conductivity values resulting from the steady state analysis is readily apparent. In contrast, the steady shape estimates are quite similar, overall, to the transient analysis estimates. Thus the steady shape approach is capable of yielding results of comparable accuracy to the transient analysis with considerably less computing (10–15 min cpu time versus 14–24 hours), while using tests of feasible duration in the field.

[31] The reason for the improvement in accuracy relative to the steady state approach is that, although a steady state simulation is not capable of accurately portraying the drawdown values themselves, it is capable of accurately portraying their differences in the region of investigation. The computed drawdowns, used in the steady state inverse analyses, are tied to the artificial outer boundary head, while the differences near the pumping well, used in the steady shape analyses, are determined by the pumping rate and geometry in conjunction with the conductivity distribution. These differences are established early in a test and remain essentially unchanged thereafter, with the region of investigation serving only as a conduit for water extracted from storage in more distant portions of the aquifer.

7. Effects of Outer Boundary Placement

[32] In order to attain true steady state conditions, the aquifer must be in contact with a source (reservoir) that is capable of supplying all the water extracted by pumping. Even if a pumping test is run to steady state, the actual mechanisms driving the system to steady state must be modeled to obtain accurate conductivity estimates. However, it is usually quite difficult to distinguish between mechanisms on the basis of the drawdown, so the boundary conditions will always be misspecified to some extent. Although such misspecification may have little noticeable effect on the drawdown response, it can have a significant effect on the estimated conductivities. Two ways of avoiding the deleterious effects of incorrectly specified boundary conditions are to perform transient analyses of early-time data, which are only marginally influenced by boundaries, or to perform steady shape analyses, since, again, the gradients in the vicinity of the pumping well are essentially insensitive to the boundaries.

[33] The insensitivity of the steady shape approach to the position of the outer boundary can be demonstrated using the same model aquifer as before. Figure 9 summarizes the error distributions resulting from both steady state and steady shape analyses of the suite of tomographic pumping tests under anistropic conditions (Kv:Kh = 1×10^{-3}) when the outer boundary in the inverse simulations is located 5163 m from the pumping well, only 45% of the distance to the "actual" outer boundary used in the generation of the drawdown data. Comparing Figure 9 to Figure 7b demonstrates that the steady shape results are largely unaffected by the misspecified outer boundary. The misspecified outer boundary, which increases the range of errors in the steady state analyses of shorter duration tests relative to the base case, generally results in a trend from enhanced overestimation for shorter test durations to underestimation for longer
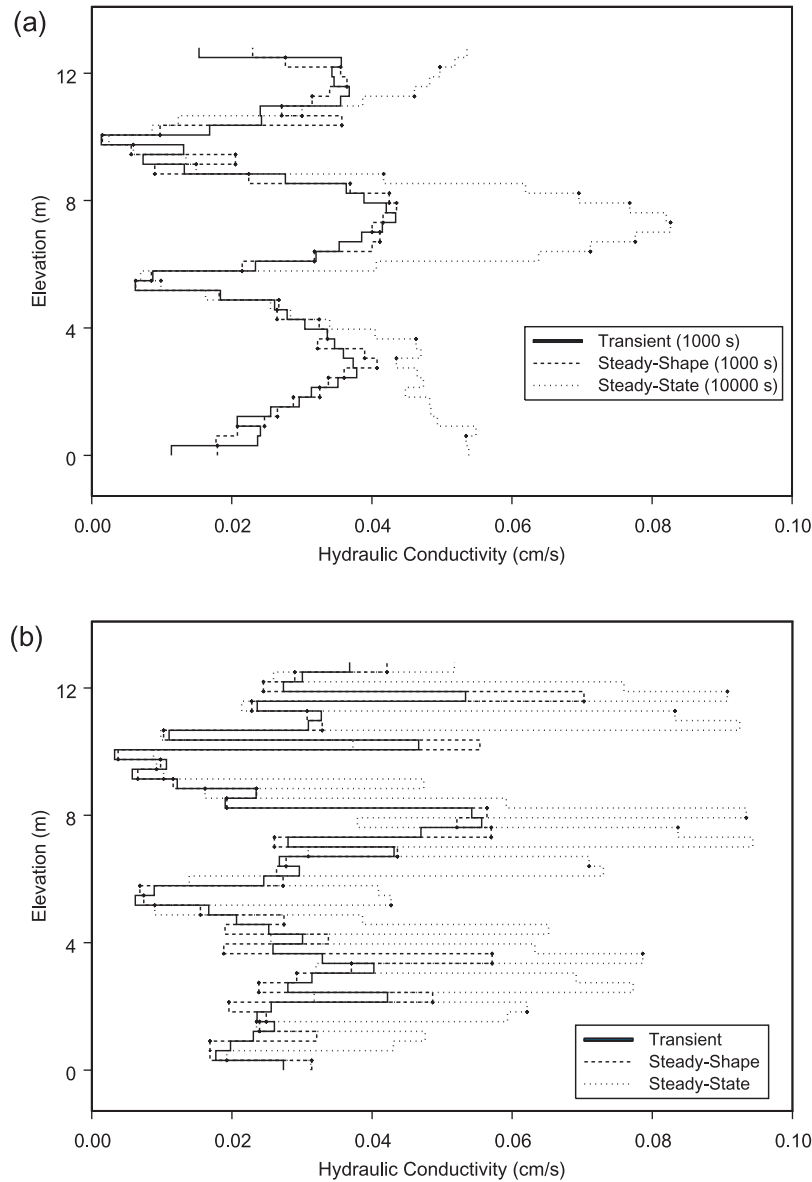
Figure 8. Estimated hydraulic conductivities for 42 layers from transient, steady state, and steady shape inversions under (a) isotropic and (b) anisotropic conditions. Most results are for test durations of 1000 s (17 min), except the steady state isotropic inversion, which failed to converge for the 1000-s test duration.

test durations. Because the zero-drawdown outer boundary used in the inverse simulations is too close to the observation points, an artificially high gradient is imposed between these points and the outer boundary at later times. Thus the conductivity estimates must be reduced to yield the proper overall flux rate. Analogous results are obtained when an outer boundary is located too far from the pumping well. In this case, the steady shape results are again largely unaffected, while the steady state results show a decided tendency toward overestimation of K, resulting from the artificially reduced gradient between the region of investigation and the outer boundary imposed by the inverse analyses.

8. Effects of Leakage

[34] Steady state conditions may also be achieved when the flux to the pumping well is balanced by leakage from an overlying or underlying unit. Like placement of an outer boundary, leakage is difficult to identify and quantify, but may have a significant impact on estimated conductivities. In order to assess that impact, we ran the same suite of tests as above, but with the addition of leakage from an overlying unit. The amount of leakage corresponded to a leakance coefficient of $B = \sqrt{Kbb'/K'} \cong 3 \times 10^3$ m in the *Hantush and Jacob* [1955] leaky aquifer function, where K and b represent the average horizontal conductivity and thickness of the aquifer and K' and b' represent the vertical conductivity and thickness of an overlying aquitard, which is presumed to separate the aquifer from an "infinite reservoir" that experiences no significant drawdown. With the addition of leakage, steady state conditions are achieved by about 10^5 s (28 hours).

[35] Figure 10 summarizes the distributions of the relative errors in the estimated conductivities when the tests are
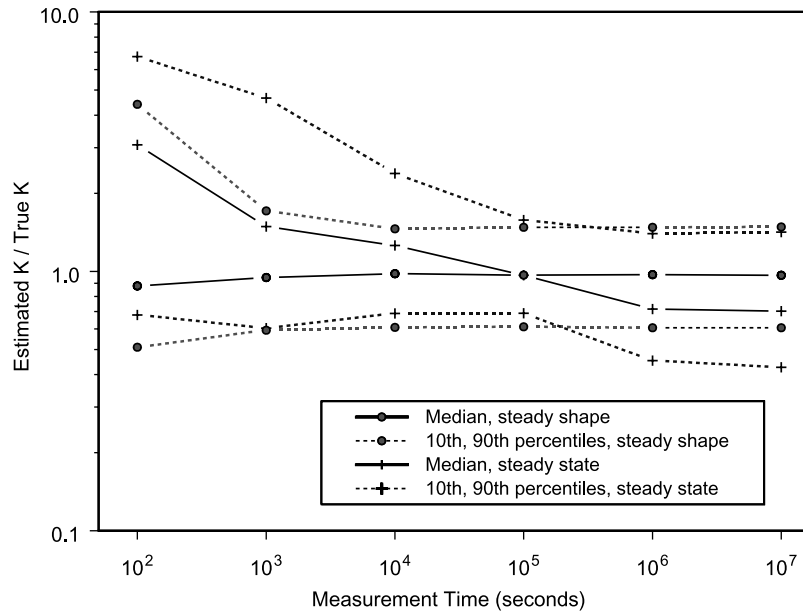
Figure 9. Summary of relative errors versus measurement time for steady state and steady shape inversions under anisotropic conditions when the outer boundary in the inverse simulations is located at 45% of the distance to the actual outer boundary.

analyzed using both steady state and steady shape methods, but ignoring the leakage in both cases. This represents a worst-case scenario in which investigators have failed to recognize the presence of leakage, a situation that would be more likely to occur in short-term tests. The leakage has greater impact under isotropic conditions than under anisotropic conditions, due to the larger vertical conductivities under isotropic conditions. The steady state inversions under isotropic conditions failed to converge due to the significant systematic error resulting from neglect of leakage, thus no results are shown for these cases. Under anisotropic conditions, the presence of leakage leads to considerably more overestimation in the steady state results, as can be seen by comparing the results shown in Figure 10b to those of Figure 7b. Leakage reduces both the lateral flux and the gradient relative to confined conditions, with the reduction increasing with distance from the pumping well. Thus the steady state analysis assumes too high a flux between the region of investigation and the outer boundary and overestimates the conductivity to compensate. Also, the actual system reaches steady state fairly rapidly due to the presence of leakage, so that the steady state estimation results stabilize fairly early, although they are incorrect due to the improper representation of the boundary conditions.

[36] Early in the tests, the leakage has little impact on the gradients in the vicinity of the pumping well, especially lower in the aquifer. Thus the steady shape analyses of data from the earlier observation times yield estimates that are quite similar to those for the base case, without leakage. Steady shape analyses of data obtained at later times show a slightly wider range of errors, due to the increased impact of leakage at these later times. The relatively small impact on steady shape conditions at all times is a result of the use of drawdown differences in the analysis. The percent of total

flow represented by the leakage between the observation wells is very small and thus has a small impact on K estimates.

9. Choice of Data Pairs

[37] The steady shape approach requires the specification of pairs of observation points between which to compute drawdown differences. This is analogous to the choice of transmitter and receiver pair locations in seismic or radar tomography. One might expect that the choice of observation point pairs would have an impact on the accuracy of hydraulic conductivity estimates in different portions of the test area. The results presented above have been based on using all possible pairs of observation points. Since there are 42 observation points for a single time, there are 861 possible drawdown differences. This set of pairs can be naturally broken down into two subsets, consisting of 588 "between-well" pairs and 273 "within-well" pairs. The within-well pairs are all of those pairs for which the two observation points are at the same radial location. The between-well pairs are the complementary subset, in which each observation point is matched only with observation points at different radial locations.

[38] The influence of data-pair specification was investigated by computing variances and covariances of the conductivity estimates resulting from different choices of data pairs. In general, the experimental design problem is nonlinear since the parameter covariance matrix depends on the parameter estimates, which in turn depend on the experimental design. However, in this case, the conductivity estimates do not change significantly for the different choices of data pairs, meaning that it is not necessary to do full inverse runs for each experimental design to estimate the parameter uncertainties that would result under each scenario. A linear
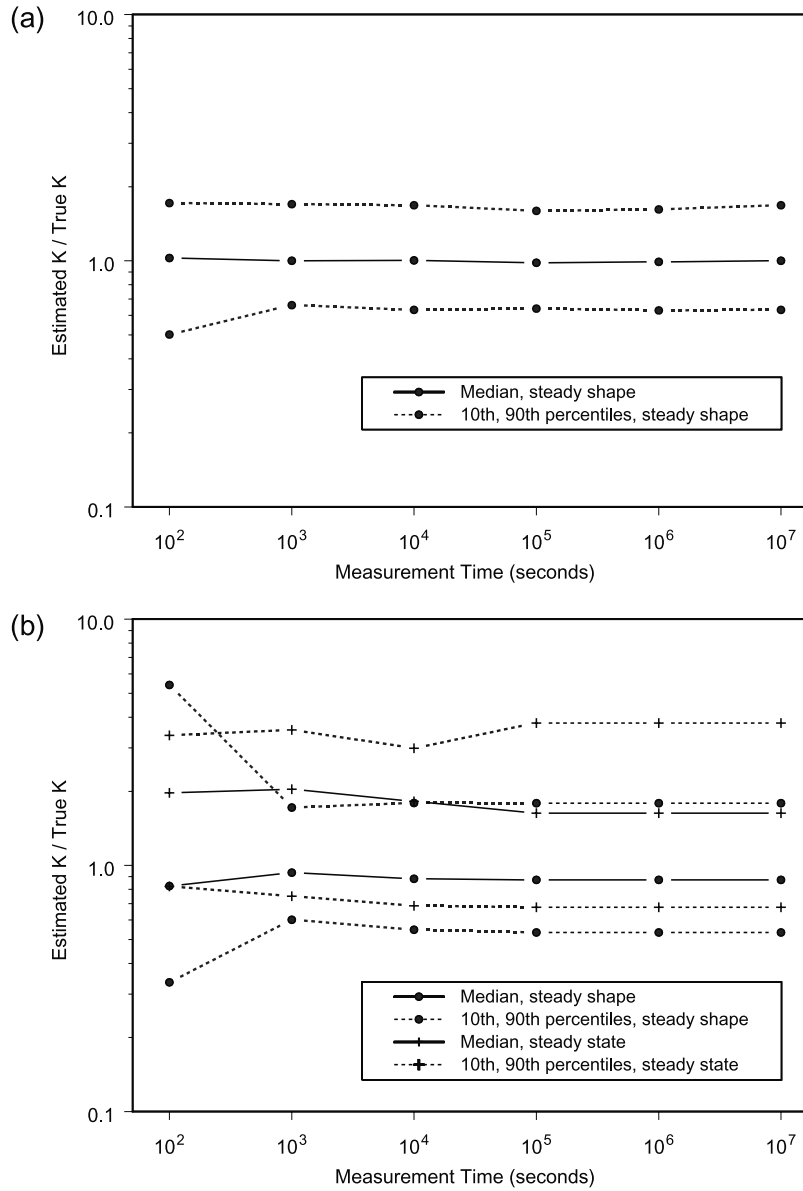
(a)

(b)

Figure 10. Summary of relative errors versus measurement time for steady state and steady shape inversions under isotropic (a) and anisotropic (b) conditions when measured drawdowns are affected by leakage which is not accounted for in inverse simulations. (Steady state inversions failed to converge under isotropic conditions.)

approximation of the parameter covariance matrix can be computed as [*Press et al.*, 1992; *Knopman and Voss*, 1988]

$$\mathbf{C} = (\mathbf{J}'\mathbf{J})^{-1} \tag{6}$$

where $\mathbf{J}$ is the Jacobian matrix, with elements given by

$$J_{i,j} = \frac{1}{\sigma_i} \frac{\partial \Delta s_i}{\partial K_j} \tag{7}$$

where K_j is the jth unknown conductivity value, Δs_i is the ith drawdown difference, and σ_i is the error standard deviation associated with Δs_i. Assuming that the drawdown measurements have normally distributed errors, then the error in Δs_i is also normally distributed, with σ_i given by

$$\sigma_i = \sqrt{\sigma_j^2 + \sigma_k^2} \tag{8}$$

where σ_j and σ_k are the error standard deviations associated with the drawdown measurements contributing to Δs_i.

[39] Figure 11 shows the coefficients of variation associated with the conductivity estimates for the 42 layers based on steady shape analysis of data collected at 1000 s under anisotropic conditions and the following three data-pair specifications: (1) all possible pairs, (2) only between-well pairs, and (3) only within-well pairs. The coefficient of variation for layer i is the standard deviation of the estimate divided by the conductivity value, given by $\sqrt{C_{ii}}/K_i$ where C_{ii} is the ith diagonal element of $\mathbf{C}$. In this case, $\mathbf{C}$ has been computed using a data standard deviation of $\sigma = 0.002$ m, a value that might be expected for drawdown measurements obtained with electronic pressure transducers. All of the coefficients of variation would scale proportionally with changes in σ, so the choice of σ is somewhat immaterial to this experimental design problem.
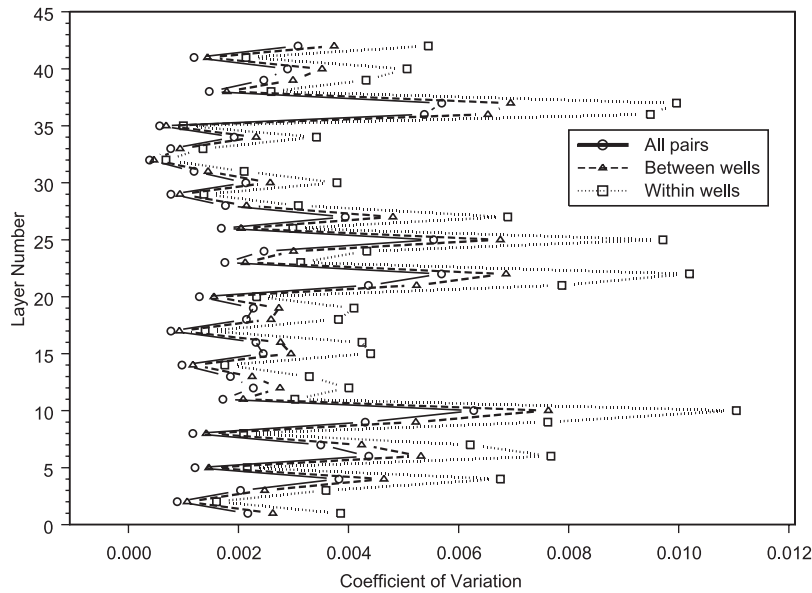
Figure 11. Coefficients of variation in hydraulic conductivity estimates versus layer number (from bottom of aquifer up) for different choices of observation pairs in steady shape inversion under anisotropic conditions.

[40] In Figure 11, the coefficient of variation for the between-well pair scenario is larger than that for the all-pair scenario by a factor of about 1.2, and that for the within-well pair scenario is about 1.8 times larger than the coefficient of variation based on all pairs. These numbers simply reflect an increase in the parameter variances in proportion to the decrease in the number of data pairs used in each analysis, implying that the change in the geometric pattern of the data pairs has had no significant influence on the results. Thus the selection of different sets of data pairs makes little significant difference in this case, perhaps because of the large number of observation points employed. To test this conjecture, the procedure was repeated using a thinned data set consisting of

only 24 observation points, shown by the filled circles in Figure 12. Based on this thinned data set, the covariance matrix of the conductivity estimates was again computed using all pairs, only between-well pairs, and only within-well pairs. The resulting coefficients of variation are shown in Figure 13. Again, the choice of different observation pairs makes little significant difference in the results, although the reduction in the number of observation points has increased the uncertainty in the conductivity estimates roughly by an order of magnitude. These results are not unexpected, given that each possible subset of drawdown differences represents a set of contrasts among a relatively small number of drawdown values and thus represents a different encoding of
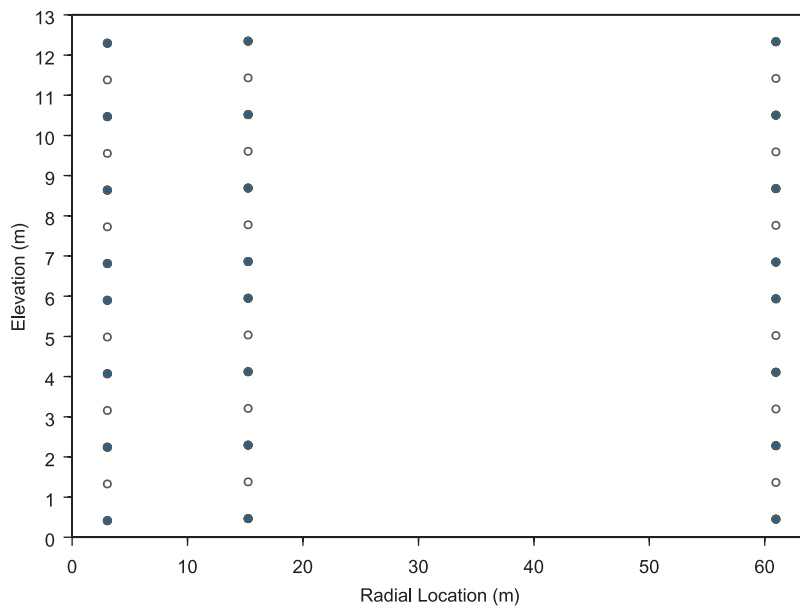

Figure 12. Filled circles show 24 observation points in thinned data set.
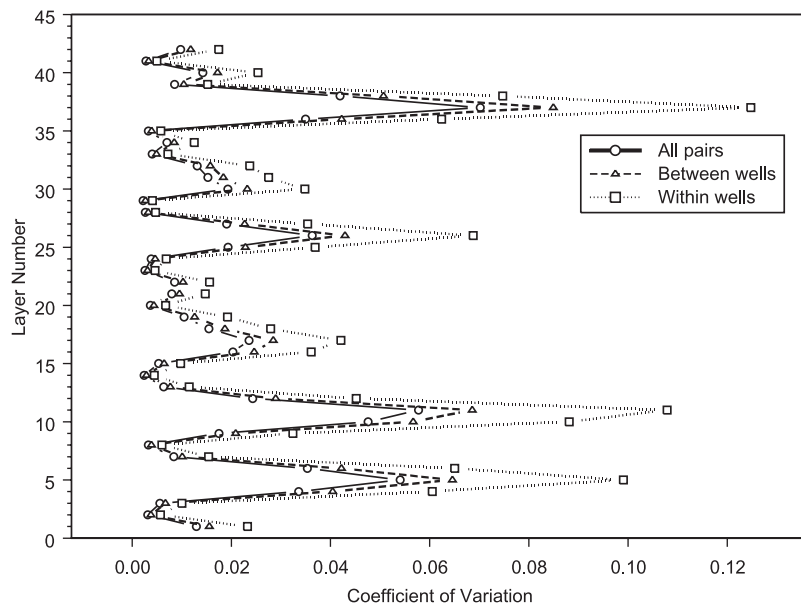
Figure 13. Coefficients of variation in hydraulic conductivity estimates versus layer number for different choices of observation pairs using thinned data set in steady shape inversion under anisotropic conditions.

essentially the same information. In fact, there is little reason not to use all drawdown differences in the analysis, since doing so represents a trivial amount of additional computation relative to the amount of time required to compute the drawdowns themselves, and the possible redundancy of information in the resulting residual vector does no harm.

10. Conclusions

[41] The steady shape approach to analysis of hydraulic tomography data retains the computational efficiency of a steady state analysis and the field practicality of transient tests, while avoiding the inaccuracies introduced by the sensitivity of a steady state analysis to an improperly specified outer boundary condition or leakage. The assumption of steady state artificially propagates the influence of boundary conditions throughout the model domain, although data may be collected well before these boundaries influence drawdown in the region of investigation. The steady shape approach focuses on gradients between observation points, which are determined primarily by the inner (pumping) boundary condition, which is known, and the conductivity distribution within the region of investigation. These gradients are rapidly established in the vicinity of the pumping well and are relatively insensitive to outer boundary conditions and leakage. Thus analysis of drawdown differences between observation points at steady shape conditions yields conductivity estimates that are essentially unaffected by the outer boundary and only marginally influenced by leakage.

[42] The purpose of this paper was to demonstrate a new approach for the analysis of hydraulic tomography data, which exploits the simplifications possible under steady shape flow conditions to greatly enhance the practical viability of the hydraulic tomography procedure. Numerical simulations with a model aquifer were used to clarify the advantages of the proposed methodology. Although these

simulations were based on a simplified depiction of aquifer heterogeneity, they clearly demonstrated the advantages of the steady shape approach. These same advantages should exist for cases involving more realistic depictions of aquifer heterogeneity. Assumptions such as the neglect of angular variations in flow properties and perfect layering, admittedly, would not be appropriate in many field settings. However, the steady shape approach can readily incorporate methods to address these limitations [e.g., *Yeh and Liu*, 2000] without compromising the efficiency of the procedure. Also, although the presence of greater hydraulic conductivity contrasts might delay the onset of steady shape conditions, due to the increased time required for low-conductivity regions to equilibrate with the surrounding medium, there is no reason why the same principles should not apply once steady shape is attained. The steady shape approach clearly enhances the practical viability of the hydraulic tomography approach, which appears to have much potential for the estimation of hydraulic conductivity variations on a scale of relevance for contaminant transport investigations.

References

Bohling, G. C., Hydraulic tomography in two-dimensional, steady-state groundwater flow, *Eos Trans. AGU*, *74*, 141, 1993.

Bohling, G. C., and J. J. Butler Jr., Lr2dinv: A finite-difference model for inverse analysis of two-dimensional linear or radial groundwater flow, *Comput. Geosci.*, *27*, 1147–1156, 2001.

Butler, J. J., Jr., Pumping tests in nonuniform aquifers—The radially symmetric case, *J. Hydrol.*, *101*(1/4), 15–30, 1988.

Butler, J. J., Jr., The role of pumping tests in site characterization: Some theoretical considerations, *Ground Water*, *28*(3), 394–402, 1990.

Butler J. J., Jr. *The Design, Performance, and Analysis of Slug Tests*, A. F. Lewis, Boca Raton, Fla., 1998.

Butler, J. J., Jr., and J. M. Healey, Relationship between pumping-test and slug-test parameters: Scale effect or artifact?, *Ground Water*, *36*(2), 305–313, 1998.

Butler, J. J., Jr., and W. Liu, Pumping tests in nonuniform aquifers: The radially asymmetric case, *Water Resour. Res.*, *29*(2), 259–269, 1993.

Butler, J. J., Jr., C. D. McElwee, and G. C. Bohling, Pumping tests in networks of multilevel sampling wells: Motivation and methodology, *Water Resour. Res.*, *35*(11), 3553–3560, 1999.

Cooper, H. H., Jr., and C. E. Jacob, A generalized graphical method for evaluating formation constants and summarizing well field history, *Eos Trans. AGU*, *27*, 526–534, 1946.

Domenico, P. A., and F. W. Schwartz, *Physical and Chemical Hydrogeology*, John Wiley, New York, 1990.

Freeze, R. A., and J. A. Cherry, *Groundwater*, Prentice-Hall, Old Tappan, N. J., 1979.

Garbow, B. S., K. E. Hillstrom, and J. J. More, The Minpack Project, Argonne Natl, Lab., Argonne, Ill., 1980.

Gottlieb, J., and P. Dietrich, Identification of the permeability distribution in soil by hydraulic tomography, *Inverse Problems*, *11*, 353–360, 1995.

Hantush, M. S., Aquifer tests on partially penetrating wells, *Proc. Am. Soc. Civ. Eng.*, *87*, 171–195, 1961.

Hantush, M. S., and C. E. Jacob, Nonsteady radial flow in an infinite leaky aquifer, *Eos Trans. AGU*, *36*, 95–100, 1955.

Heath, R. C., and F. W. Trainer, *Introduction to Groundwater Hydrology*, John Wiley, New York, 1968.

Jacob, C. E., Determining the permeability of water-table aquifers, in *Methods of Determining Permeability, Transmissibility, and Drawdown*, compiled by R. Bentall, *U.S. Geol. Surv. Water Supply Pap.*, *1536-I*, 245–271, 1963.

Knopman, D. S., and C. I. Voss, Further comments on sensitivities, parameter estimation, and sampling design in one-dimensional analysis of solute transport in porous media, *Water Resour. Res.*, *24*(2), 225–238, 1988.

Kruseman, G. P., and N. A. de Ridder, Analysis and evaluation of pumping test data, *ILRI Pub. 47*, Int. Inst. for Land Reclamation and Improvement, Wageningen, Netherlands, 1989.

Marquardt, D. W., An algorithm for least squares estimation of non-linear parameters, *J. Soc. Ind. Appl. Math.*, *2*, 431–441, 1963.

Meier, P. M., J. Carrera, and X. Sanchez-Vila, An evaluation of Jacob's method for the interpretation of pumping tests in heterogeneous formations, *Water Resour. Res.*, *34*(5), 1011–1025, 1998.

Oliver, D. S., The influence of nonuniform transmissivity and storativity on drawdown, *Water Resour. Res.*, *29*(1), 169–178, 1993.

Peterson, J. E., B. N. P. Paulsson, and T. V. McEvilly, Application of algebraic reconstruction techniques to crosshole seismic data, *Geophysics*, *50*(10), 1566–1580, 1985.

Press, W. H., S. A. Teukolsky, W. T. Vetterling, and B. P. Flannery, *Numerical Recipes in FORTRAN: The Art of Scientific Computing*, 2nd ed., Cambridge Univ. Press, New York, 1992.

Shapiro, A. M., Interpretation of oscillatory water levels in observation wells during aquifer tests in fractured rock, *Water Resour. Res.*, *25*(10), 2129–2137, 1989.

Theis, C. V., The source of water derived from wells, *Civ. Eng.*, *10*(5), 277–280, 1940.

Tosaka, H., K. Masumoto, and K. Kojima, Hydropulse tomography for identifying 3-d permeability distribution, in *High Level Radioactive Waste Management: Proceedings of the Fourth Annual International Conference of the ASCE*, pp. 955–959, Am. Soc. of Civ. Eng., Reston, Va., 1993.

Vasco, D. W., J. E. Peterson Jr., and K. H. Lee, Ground-penetrating radar velocity tomography in heterogeneous and anisotropic media, *Geophysics*, *62*(6), 1758–1773, 1997.

Vasco, D. W., H. Keers, and K. Karasaki, Estimation of reservoir properties using transient pressure data: An asymptotic approach, *Water Resour. Res.*, *36*(12), 3447–3465, 2000.

Wenzel, L. K., Methods for determining permeability of water-bearing materials, with special reference to discharging-well methods, *U.S. Geol. Surv. Water Supply Pap., 887*, 192 pp., 1942.

Yeh, T.-C. J., and S. Liu, Hydraulic tomography: Development of a new aquifer test method, *Water Resour. Res.*, *36*(8), 2095–2105, 2000.

Yeh, T.-C. J., J. Mas-Pla, T. M. Williams, and J. F. McCarthy, Observation and three-dimensional simulation of chloride plumes in a sandy aquifer under forced-gradient conditions, *Water Resour. Res.*, *31*(9), 2141–2157, 1995.

———————————

G. C. Bohling, J. J. Butler Jr., X. Zhan, and L. Zheng, Kansas Geological Survey, 1930 Constant Avenue, Campus West, University of Kansas, Lawrence, KS 66047, USA. (geoff@kgs.ukans.edu)
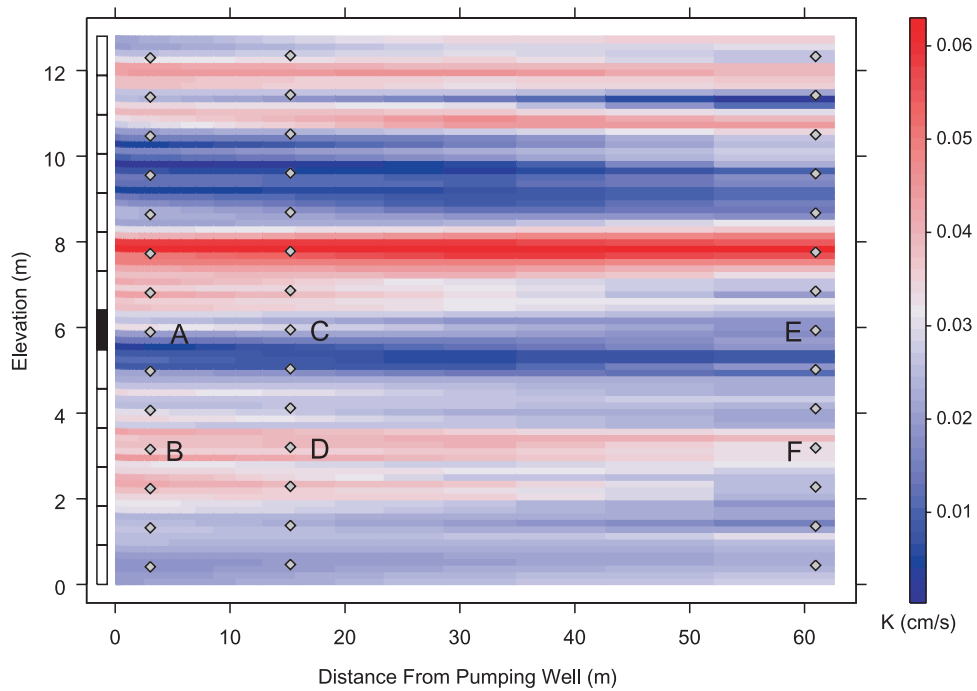
Figure 3. True conductivity distribution out to 62 m radial distance from pumping well. Boxes on left indicate pumping intervals for 14 tests, with interval for test 7 highlighted. Diamonds represent observation points. Drawdowns at points A–F are shown in following figures.
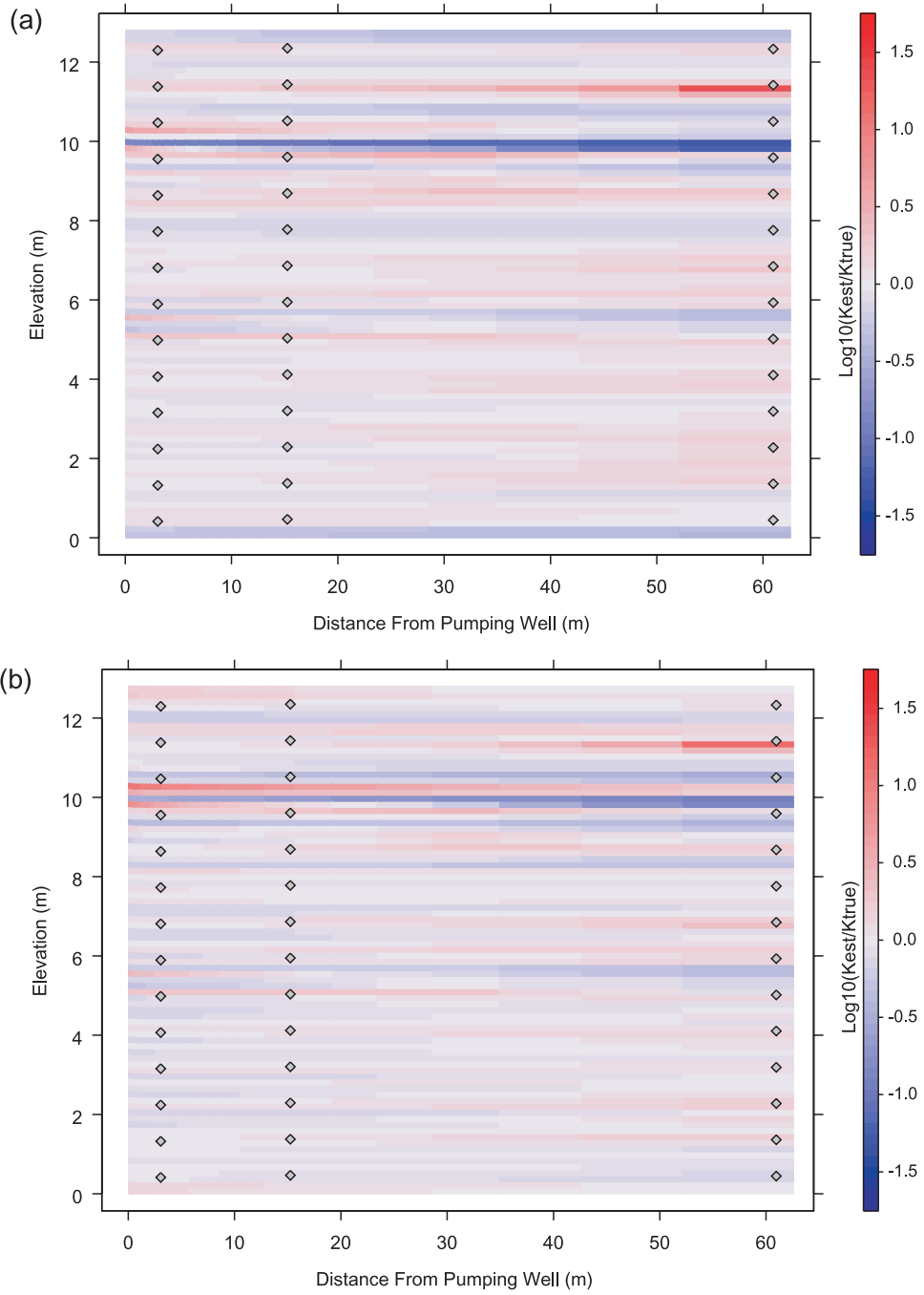
Figure 6. Relative error from transient inversions under (a) isotropic and (b) anisotropic conditions, represented in terms of the base 10 logarithm of estimated versus true conductivity in each cell of the forward model grid.